SCIEPublish

Article

High-Temperature Dielectric Energy Storage Materials Fabricated by Crosslinking Titanium Dioxide and Polyarylene Ether Nitrile

Yujie Feng, Shumin Bao, Zaixing Wang, Yongxian Liu, Yayao Jiao, Lingling Wang *, Xiufu Hua * and Renbo Wei *

School of Chemical Engineering, Northwest University, Xi'an 710069, China; fengyujie01@qq.com (Y.F.); baoshumin@stumail.nwu.edu.cn (S.B.); wangzaixing@stumail.nwu.edu.cn (Z.W.); liuyongxian@stumail.nwu.edu.cn (Y.L.); jiaoyy@stumail.nwu.edu.cn (Y.J.)

* Corresponding author. E-mail: wangll@nwu.edu.cn (L.W.); huaxf@nwu.edu.cn (X.H.); weirb10@nwu.edu.cn (R.W.)

Received: 7 February 2025; Accepted: 5 June 2025; Available online: 9 June 2025

ABSTRACT: Dielectric materials have broad application prospects in the field of high-temperature electronic power systems. Up to now, high-temperature dielectric materials are mainly prepared by using high glass transition temperature (T_g) polymers. However, the incompatibility between polymers and fillers, which are incorporated for high energy density, leads to soaring dielectric losses at high temperatures, resulting in a nosedive of discharged energy density (U_d) and efficiency (η). In this paper, we report the fabrication of high-temperature dielectric materials via the self-crosslinking of phthalonitriles from phthalonitriles modified titanium dioxide (TiO_2-2CN) and phthalonitriles terminated polyarylene ether nitrile (PEN-2CN). TiO_2-2CN is firstly synthesized and characterized, then incorporated into PEN-2CN to prepare TiO_2/PEN nanocomposites, which transform into TiO_2-PEN hybrids afterwards. The fabricated TiO_2-PEN hybrids are confirmed by the change of SEM sectional morphology, as well as the increase of their T_g and thermal decomposition temperature (T_d). With the addition of TiO_2-2CN, both the T_g, T_d, and U_d of TiO_2/PEN nanocomposites are improved. In addition, due to the formation of covalent bonds within TiO_2-PEN, the hybrids exhibit excellent high-temperature dielectric energy storage performance. Specifically, at 150 °C, the U_d of 10 wt% TiO_2-PEN is 0.60 J/cm^{-3}, which is over 95% of that at RT. Moreover, η is greater than 90% and remains unchanged after 10,000 charge and discharge cycles. This method used for preparing TiO_2-PEN hybrids through a self-crosslinking reaction of phthalonitriles provides a new approach for preparing high-temperature dielectric materials.

Keywords: Dielectric materials; Energy density; High-temperature; Crosslinking

1. Introduction

Electric energy storage devices are essential electronic components in fields such as advanced microelectronics, electric vehicles, and aerospace [1]. Among them, dielectric capacitor, which stores electrical energy in the form of electrostatic fields, are widely used, resulting from their rapid charging and discharging speed, eminent power density, and excellent reliability [2]. Dielectric capacitors can typically be divided into ceramic capacitors and polymer thin film capacitors [3]. The ceramic dielectric materials have relatively high dielectric constant, but they also exhibit disadvantages such as low breakdown strength, high processing temperature, and brittleness [4]. With the development of capacitors towards miniaturization and lightweight, More and more attention has been paid to polymeric dielectric capacitors [5–8]. Polymer dielectrics not only have the advantages of lightweight, easy processing, and high breakdown strength but also demonstrate many unique advantages, covering low price, mechanical flexibility, and strong charge-discharge cycling ability [9]. However, the relatively low operating temperature of polymers limits their further applications. For example, the widely used biaxially oriented polypropylene (BOPP) exhibits ultra-high breakdown strength at room temperature, but its breakdown strength sharply decreases when the working temperature exceeds 105 °C, which cannot meet the high-temperature requirements of aerospace, hybrid vehicles, oil and gas exploration and other fields [10]. Therefore, it is urgent to develop polymer based dielectric materials with excellent energy storage performance to meet the high-temperature application needs of electronic power systems.

https://doi.org/10.70322/htm.2025.10010

In order to meet the operation requirements of contemporary high-power electronic devices at high temperatures, a series of super engineering plastics showing high glass transition temperature (T_g) have been developed [11,12]. Resulting from the abundant aromatic groups or condensed heterocyclic rings on the main chain, these polymers have high thermal and mechanical stability [13]. Typical representatives include phenylene sulfide (PPS) [14], poly(arylene ether ketone) (PEK) [15], poly(arylene ether nitrile) (PEN) [16], poly(arylene ether urea) (PEEU) [17], polyetherimide (PEI) [18,19], polyimide (PI) [20], *etc.* [21–23]. Among them, PEN is a structurally regular linear semi-crystalline polymer with cyanide groups at the side chain and aromatic ether bonds in the main chain [24]. The aromatic ether bond in its main chain enables it to reach a T_g higher than 150 °C. On the other hand, the presence of cyanide endows it with a high dielectric constant, a prerequisite for high energy storage density [25]. Additionally, the cyanide group at the side chain of PEN also gives it excellent processing and molding ability. Compared to materials such as PI, PEN can be melted or solution processed, which demonstrates promising application in fields such as military defense, the microelectronics industry, electronic circuits, automobile manufacturing, aircraft manufacturing, and petrochemicals [26].

Crosslinking is another effective method to improve the thermal stability of polymer dielectrics [27]. On one hand, it restricts the movement and polarization of polymer segments, thus enhancing thermal stability [28]. On the other hand, it elevates breakdown strength, thereby improving the energy storage performance [29]. Most crosslinking processes require the addition of crosslinking agents, while the residue crosslinking agents would depress the energy storage performance. In addition, the released gas and/or small molecule substances during crosslinking could also affect the energy storage performance [30,31]. Therefore, a suitable crosslinking reaction is important for preparing high-temperature dielectric materials. Accordingly, Zhang and coauthors [32] fabricated a series of crosslinked PEI having different crosslinking degrees by adjusting the crosslinking reaction of phenylacetylene groups. When the gel content reaches 35 wt%, and the molecular weight of the soluble chain is about 6×10^4, the discharged energy density exceeds 3.60 J/cm^3 at 150 °C with an efficiency that remains above 95%. Our previous researches show that phthalonitriles can undergo self-crosslinking reactions at high temperatures, forming phthalocyanine rings without releasing small molecules [33,34]. Basing on this reaction, high-temperature dielectrics with a T_g higher than 350 °C have been successfully prepared from phthalonitriles modified BN and CNT, as well as phthalonitriles capped PEN [35].

In this work, TiO_2 and PEN hybrid materials are prepared via the self-crosslinking of phthalonitriles, and act as high-temperature dielectrics. To improve the thermal stability of these dielectrics, a cross-linkable PEN terminated with phthalonitriles is first prepared. Subsequently, phthalonitriles modified TiO_2 is introduced into the cross-linkable PEN matrix by grafting phthalonitriles on the surface of TiO_2. After self-crosslinking at high temperatures, TiO_2-PEN hybrids are successfully obtained. Results show that the TiO_2-PEN hybrids can be used as a high-temperature dielectrics due to their long-term use at 150 °C.

2. Experimental Section

2.1. Materials

TiO_2 (20–30 nm) was provided by Tianjin Kemier. 4-Nitrophthalonitrile (4-NPh) biphenyldiol (BP) and dichlorobenzonitrile (DCBN), and hydroquinone (HQ) were purchased from Shanghai Macklin Biochemicals. Hydrogen peroxide (H_2O_2), N-methylpyrrolidone (NMP) and N,N-dimethylformamide (DMF) were obtained from local suppliers. PEN terminated with phthalonitriles was synthesized according to the reference [36]. Other chemicals were commercially available products and used directly.

2.2. Synthesis of Phthalonitriles Modified TiO_2 (TiO_2-2CN)

TiO_2-2CNwas synthesized according to the literature [37]. Specifically, 5.0 g TiO_2 was added into H_2O_2 (0.25 L), then heated to reflux for 4 h upon stirring. After centrifugal separation and washing with deionized water for 3 times, TiO_2-OH was synthesized via drying at 80 °C for 12 h in a vacuum. This obtained TiO_2-OH (1.0 g) and 4-NPh (1.0 g) were added into DMF (250 mL) with the existence of potassium carbonate (1.0 g). This blend was heated to reflux with stirring overnight. After the reaction, the crude product was centrifuged and then washed with DMF and water each for 3 times. TiO_2-2CN was finally obtained via drying at 100 °C overnight in a vacuum.

2.3. Preparation of TiO_2/PEN Nanocomposites

The TiO_2/PEN nanocomposites were prepared by using the solution casting method. Firstly, a certain amount of TiO_2-2CN and PEN-2CN were added to 10 mL of NMP, and stirred at 60 °C for 2 h. The obtained homogeneous mixture

was then cast onto a clean glass plate and heated in a program-controlled blast oven. After removing the solvent, TiO_2/PEN nanocomposite films with a thickness of approximately 50 μm were separated from the glass plate. TiO_2/PEN nanocomposite films with TiO_2-2CN contents of 0, 5, 10, 15, and 20 wt% were prepared by controlling the dosage of TiO_2-2CN and PEN-2CN.

2.4. Fabrication of TiO_2-PEN Hybrids

TiO_2-PEN hybrid films were fabricated via the self-crosslinking reaction of phthalonitriles by treating the TiO_2/PEN nanocomposite film in a 320 °C muffle furnace for 4 h. Basing on the content of TiO_2-2CN in TiO_2/PEN nanocomposites, the hybrids were named 0, 5, 10, 15, and 20 wt% TiO_2-PEN, respectively.

2.5. Characterization

FTIR spectra of TiO_2, 4-NPh and TiO_2-2CN were collected using a Nicolet 200SXV instrument (Thermofisher, Madison, WI, USA). The crystalline structures of TiO_2 and TiO_2-2CN were measured by D8 Advance XRD (Bruker, Karlsruhe, Germany) using Cu Kα radiation. XPS (Escalab 250xi, Thermofisher, Madison, WI, USA) with an Al Kα X-ray source was used to test the band structure of TiO_2-2CN. Micro-morphology of TiO_2, nanocomposite films and hybrid films were tested using TESCAN MIRA4 (Brno, Czech) field emission scanning electron microscopy (SEM) with an acceleration voltage of 15 kV. Dielectric performance was tested using a TH2826 LCR meter (Tong Hui, Changzhou, China). Breakdown strength of the samples was tested with a ZJC-5 kV withstand voltage tester (Zhonghang, Beijing, China). The thermal properties of the samples were obtained by TGA (HTG-1, Beijing Hengjiu, Beijing, China) and DSC (DSC-1, Beijing Hengjiu, Beijing, China) in a nitrogen environment. The polarization electric field (P-E) loops of TiO_2/2CN and TiO_2-2CN were measured using a ferroelectric tester (Premiere II, Radiant Technologies, Alpharetta, GA, USA) at a frequency of 1000 Hz. The simulation of the breakdown process of the thin film was conducted via finite element analysis using COMSOL Multiphysics 6.2, with detailed information in the Supplementary Materials.

3. Results and Discussions

In this study, high-temperature dielectrics TiO_2-PEN hybrids are fabricated through self-crosslinking reaction of phthalonitriles from TiO_2-2CN and PEN-2CN. Firstly, PEN-2CN terminated with phthalonitriles (Figure 1a) is prepared. Simultaneously, phthalonitrile groups are grafted onto the surface of TiO_2 to obtain TiO_2-2CN (Figure 1b). TiO_2/PEN nanocomposites are then prepared from TiO_2-2CN and PEN-2CN using the solution casting method. Finally, the nanocomposites TiO_2/PEN are treated at high temperatures to induce self-crosslinking reaction of phthalonitriles, resulting in the high-temperature dielectrics TiO_2-PEN hybrids (Figure 1c).

PEN-2CN was prepared according to the literature [36]. TiO_2-2CN was synthesized via a two-step procedure, which includes the hydroxylation of TiO_2 and a reaction with 4-NPh [37]. Figure 2a shows the FTIR spectra of TiO_2, 4-NPh and TiO_2-2CN. TiO_2 exhibits infrared absorption peaks at 3435 and 1628 cm^{-1}, which are derived from crystallization water and hydroxyl groups at the periphery of TiO_2, respectively [38]. As an organic compound, 4-NPh exhibits a series of peaks, including at 2227 cm^{-1} (cyano group), 1618–1514 cm^{-1} (benzene ring) and 1352 cm^{-1} (C-H) on benzene [39]. After the two-step reaction, the absorption peak of TiO_2-2CN at 3435 cm^{-1} becomes wider, indicating that there are more hydroxyl groups that are formed during the hydroxylation process. In addition, peaks appear at 2227, 1628, 1352, and 1299 cm^{-1} suggesting that phthalonitriles have been grafted onto its surface. Figure 2b is the TGA curves of TiO_2 and TiO_2-2CN. TiO_2 exhibits a mass reduction of less than 2.0 wt% from 80–800 °C, which would be due to the loss of surface crystalline water. In contrast, the residual mass of TiO_2-2CN at 800 °C is only 90.6 wt%. Therefore, it can be calculated that the grafting ratio of phthalonitriles on TiO_2-2CN is 7.6 wt% [40].

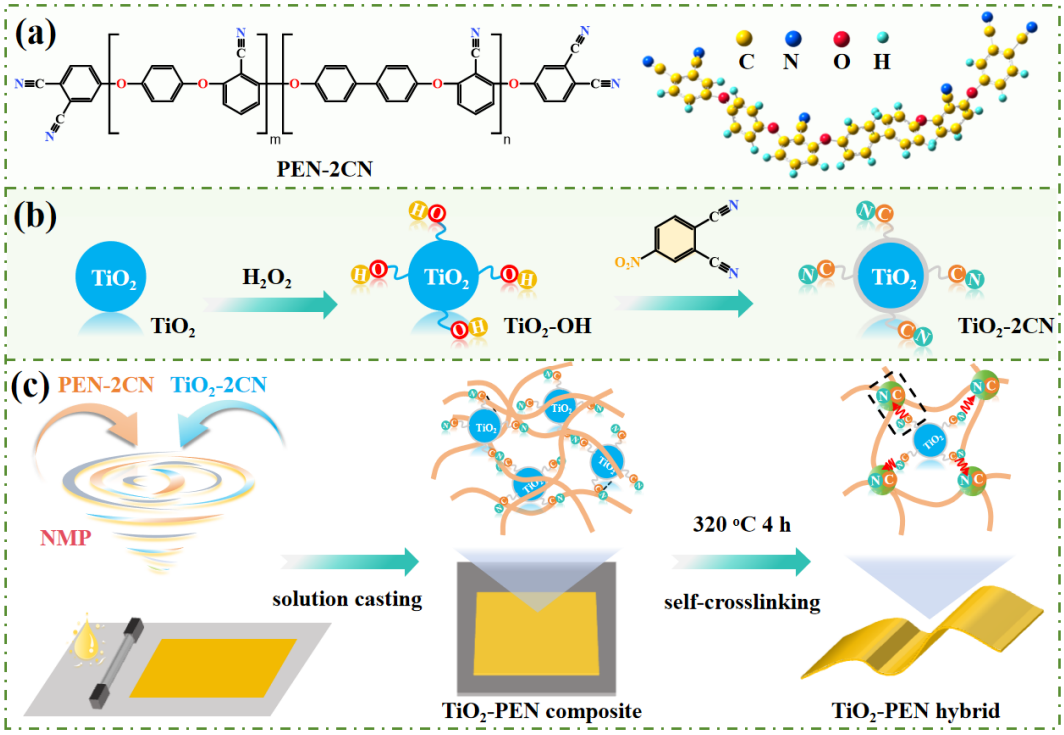

Figure 1. (**a**) Structure of PEN-2CN; (**b**) preparation procedures for TiO_2-2CN; (**c**) scheme for the fabrication of TiO_2-PEN hybrids.

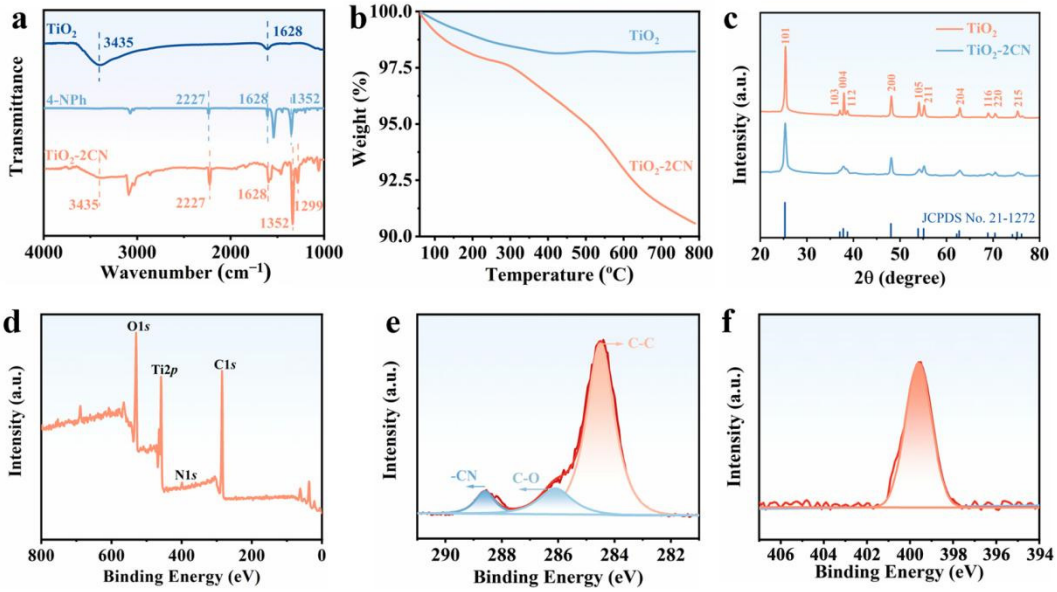

Figure 2. (**a**) FTIR spectra, (**b**) TGA curves and (**c**) XRD patterns of TiO_2 and TiO_2-2CN; (**d**) XPS, (**e**) XPS C1s and (**f**) XPS N1s spectrum of TiO_2-2CN.

The composition of TiO_2-2CN was also characterized via XPS. As displayed by Figure 2d, the XPS full spectrum of TiO_2-2CN displays elements including O (530.0 eV), Ti (460.0 eV), N (402.2 eV), and C (285.0 eV), respectively, indicating the existence of organic and inorganic components. The XPS C1s spectrum can be further decomposed into peaks at 288.6, 286.1 and 284.5 eV, corresponding to -C≡N, C-O, and C-C, respectively (Figure 2e) [41]. In addition, the XPS N1s spectrum shows a single -C≡N peak at 399.6 eV (Figure 2f) [42]. The XPS results are consistent with the structure of TiO_2-2CN, indicating the successful grafting of phthalonitriles. Finally, the structure of TiO_2-2CN was confirmed by XRD. As depicted in Figure 2c, TiO_2 demonstrates diffraction peaks at 25.28, 37.80, 48.05, 53.89, 55.06, 62.69, 68.87, 70.39, 74.15, 75.15, and 76.12°, corresponding to crystal planes of (101), (004), (200), (105), (211), (204), (116), (220), and (215), respectively. This result is consistent with the published standard card of JCPDS No. 21-1272, indicating an anatase type TiO_2 [43]. In contrast, the XRD diffraction peaks of TiO_2-2CN become wider after grafting of phthalonitriles, while their position is maintained, suggesting the same crystalline structure of TiO_2.

The micro-morphology of TiO_2 and TiO_2-2CN was further studied by SEM and TEM observation. Figure 3a,b shows SEM images of TiO_2, revealing numerous individual particles with a particle size of approximately 20 nm. In contrast, after surface modification, TiO_2-2CN appears to be stuck together with similar particle sizes (Figure 3e). In addition, Figure 3f is the SEM mapping images of TiO_2-2CN. C, N, Ti and O elements can be clearly identified from these figures. Figure 3c,d is TEM images of TiO_2 and TiO_2-2CN. The blurred boundaries on the surface of TiO_2-2CN particles indicate that their surfaces have been modified. All of the above results indicate that TiO_2-2CN has been successfully prepared. Subsequently, the synthesized TiO_2-2CN was incorporated into PEN-2CN to prepare TiO_2/PEN nanocomposites, which transform into TiO_2-PEN hybrids afterwards. Figure 3g shows the cross-section morphology of PEN-2CN, from which some fracture marks can be observed, indicating its tough nature [44]. The fracture marks scale up and form fish-scale-like cracks after the incorporation of TiO_2-2CN (Figure 3i). Moreover, TiO2-2CN is homogeneously dispersed in the polymer matrix even at the filler content of 20 wt%. This would be resulted from the surface modification of TiO_2-2CN, which exhibits excellent compatibility with PEN, and can be confirmed by the corresponding SEM mapping images in Figure 3j [45]. Figure 3h is the SEM cross-section morphology of PEN-2CN after self-crosslinking (0 wt% TiO_2-PEN). Compared to that of PEN-2CN, the cross-section is denser and neater, suggesting a brittle fracture. The brittle fracture is caused by the self-crosslinking reaction of phthalonitriles in PEN-2CN, which transforms the system from a thermoplastic system to a thermosetting network [46]. Similar phenomena are also observed in the cross-sectional view of the other hybrids containing fillers. For example, no fish-scale-like crack is observed in the hybrid 10 wt% TiO_2-PEN, but there is a brittle fracture morphology (Figure 3k). Additionally, compared with the plenty of TiO_2-2CN particles observed aside from the fish-scale-like cracks in 10 wt% TiO_2/PEN, there is not any obvious nanofiller that can be seen from the cross-section of 10 wt% TiO_2-PEN. The result is a consequence of the formed covalent bonds between TiO_2 and PEN. As the organic part is easier to break during liquid nitrogen brittling, TiO_2 would be encapsulated beneath the cross-section. Nevertheless, the TiO_2-PEN hybrid still demonstrates excellent flexibility and can be cyclically bent without breaking, as depicted in Figure 3l.

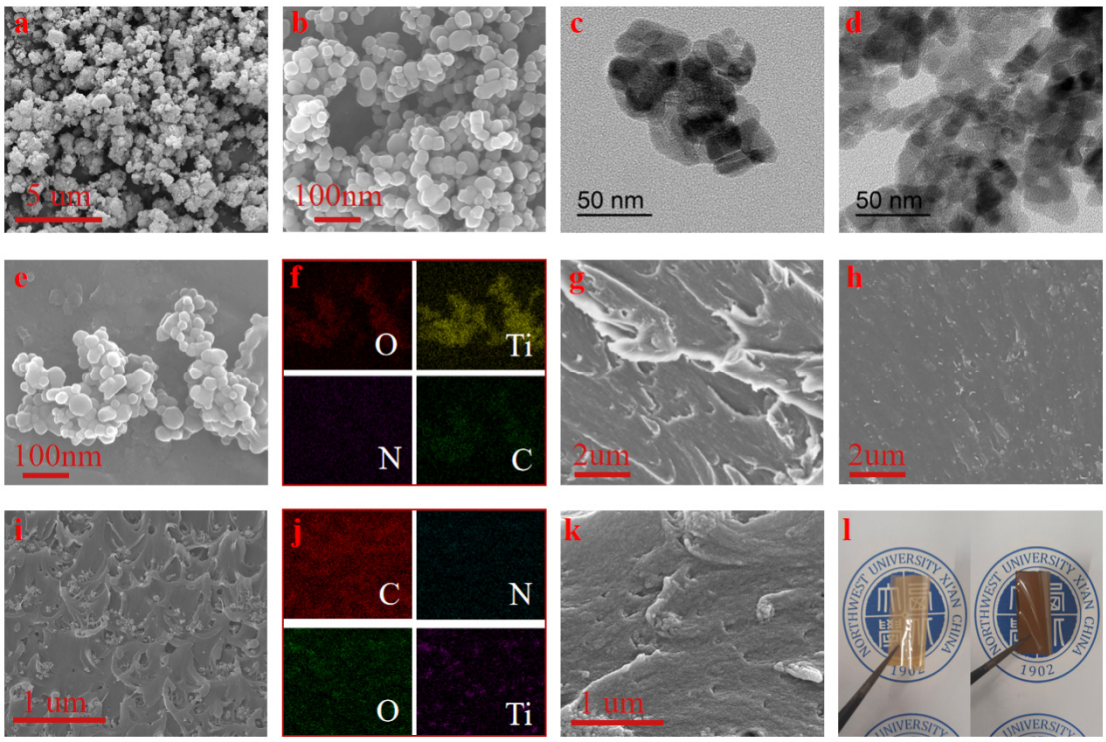

Figure 3. SEM (**a**,**b**) and TEM (**c**) images of TiO_2; TEM (**d**), SEM (**e**) and SEM mapping images (**f**) of TiO_2-2CN; SEM image of 0 wt% TiO_2/PEN (**g**), 0 wt% TiO_2-PEN (**h**), 10 wt% TiO_2/PEN (**i**) and 10 wt% TiO_2-PEN (**k**); SEM mapping images of 10 wt% TiO_2/PEN (**j**); (**l**) photographs of 10 wt% TiO_2/PEN and 10 wt% TiO_2-PEN.

The transition of TiO_2/PEN nanocomposites into TiO_2-PEN hybrids can also be confirmed by their thermal and mechanical properties. Figure S1 shows the DSC heating curves of TiO_2/PEN nanocomposites. The T_g of 0 wt% TiO_2/PEN is 195.4 °C, and the T_g increases gradually as the filler content augments to 20 wt%. For comparison, the T_g of TiO_2-PEN hybrids is higher than that of TiO_2/PEN nanocomposite. This is because these TiO_2-PEN hybrids are cross-linked networks in which the movement of polymer segments is restricted (Figure S2) [47]. Similar results can

also be obtained from the TGA curves of TiO_2/PEN and TiO_2-PEN. As shown in Figures S3 and S4, the residual mass of 0 wt% TiO_2/PEN at 800 °C is 60.1 wt%, while it is 66.3 wt% for 0 wt% TiO_2-PEN due to its crosslinked structure. Naturally, attributing to the relatively high residual mass of TiO_2-2CN, the residual mass of both TiO_2/PEN and TiO_2-PEN at 800 °C increases gradually. Moreover, the crosslinking of TiO_2-PEN hybrids is also certified by their augmented thermal decomposition temperature ($T_{10\%}$). The $T_{10\%}$ of TiO_2-PEN hybrids is not only higher than that of TiO_2/PEN nanocomposites but also increases obviously with the increase of filler content (Tables S1 and S2). With the increasing of TiO_2-2CN content, the number of phthalonitrile groups that can undergo self-crosslinking reaction increases, which leads to an augment in crosslinking density in TiO_2-PEN hybrids and thus enhances their $T_{10\%}$ [48]. Figures S5–S10 are the mechanical properties of TiO_2/PEN and TiO_2-PEN. Compared with TiO_2/PEN nanocomposites, TiO_2-PEN hybrids demonstrate higher tensile strength and modulus but lower elongation at break at the same filler content, which is consistent with the fact that TiO_2-PEN is self-crosslinked from TiO_2/PEN. Interestingly, the tensile strength and modulus of 5 wt% TiO_2-PEN reach the crest values of 115.3 MPa and 2277 MPa, which can be explained from two aspects: on one hand, the tensile strength and modulus are improved after crosslinking, and the amount of improvement is affected by the crosslinking density; on the other hand, at the increased filler concentration, both of tensile strength and modulus decrease gradually. The combination of these effects results in the peak values at the filler content of 5 wt% [49].

After the preparation of TiO_2/PEN and TiO_2-PEN, their dielectric properties were investigated in detail. Figure 4a exhibits the dielectric constant variation of TiO_2/PEN with frequency. Firstly, it can be seen that the dielectric constant of TiO_2/PEN increases gradually as TiO_2 content increases. Specifically, at 1 kHz, it increases from 3.86 for 0 wt% TiO_2/PEN to 4.72 for 20 wt% TiO_2/PEN (Table S1). Moreover, the dielectric constant of each TiO_2/PEN composite decreases with the increased frequency. This could be explained by the effect of polarization relaxation, which is always observed in the system with higher filler content [50]. Nevertheless, the dielectric constant of TiO_2/PEN is stable as the highest variation of dielectric constant with frequency is just 3.7×10^{-7} °C^{-1} from 100 Hz to 1 MHz. Similar phenomena are also obtained for the dielectric constant of TiO_2-PEN (Figure 4b). However, due to the crosslinked system, the dielectric constant and its variation values are lower than those of TiO_2/PEN at the same filler concentration, as demonstrated by Figure 4c. Dielectric loss of TiO_2/PEN and TiO_2-PEN exhibit the same result as that of dielectric constant (Figures S11 and S12), as reported in the literature [50]. Figure 4d depicts the Weibull distribution of the breakdown strength of TiO_2/PEN [51]. It is obvious that the breakdown strength of TiO_2/PEN decreases gradually as the filler content increases. This is a results of the interface incompatibility between inorganic fillers and polymer matrix, which exacerbates the distortion of the electric field. In order to further investigate the breakdown process of dielectrics, finite element analysis based on COMSOL Multiphysics 6.2 was conducted. The calculation adopts the phase field dielectric breakdown model developed by Hong and coworkers, which is described in the supporting information [52]. Figure 5 demonstrates the simulated breakdown process of PEN-2CN, 10 wt% TiO_2/PEN, and 10 wt% TiO_2-PEN at different times, respectively. The formation process of the electric tree can be easily recognized from the figures. Comparing with pure PEN-2CN, the breakdown strength of TiO_2/PEN decreases with the increase of filler content due to the fact that the interfaces between TiO_2 and PEN are easier to break down. In addition, the electric breakdown tree of 10 wt% TiO_2-PEN is bigger than that of 10 wt% TiO_2/PEN at 4 s, which is consistent with the result of the breakdown strength shown in Figure 4e. There are literature reports that the breakdown strength increases after crosslinking [53]. Consequently, the decreasing breakdown strength of TiO_2-PEN from TiO_2/PEN could be attributed to the formation of conjugated phthalocyanine rings from the self-crosslinking of phthalonitriles. The conjugated phthalocyanine rings can serve as conductive points in the system, which is suitable for the passing of electric trees and results in the abating of the breakdown strength of TiO_2-PEN (Figure 4f) [54]. The P-E loops of TiO_2/PEN and TiO_2-PEN were further tested to investigate their energy storage performance. The maximum electric field of the P-E loops was set to be 180 kV/mm, due to the 194.3 kV/mm breakdown strength of 20 wt% TiO_2-PEN (Figure 4g,h). According to the P-E loops, it can be concluded that both TiO_2/PEN and TiO_2-PEN are linear dielectrics [55]. Additionally, the discharged energy density (U_d, Figure 4i) and efficiency (η, Figure S13) of TiO_2/PEN and TiO_2-PEN can be obtained via integrating these lines (Tables S1 and S2) [55]. With the increase of TiO_2-2CN content, U_d of both TiO_2/PEN and TiO_2-PEN increases. Basing on literature, U_d of linear dielectrics is related to their dielectric constant and breakdown strength [56]. Thereby, the increased U_d is determined by the increased dielectric constant as the electric field strength is 180 kV/mm. In addition, it can be obtained from Table S2 that U_d of TiO_2-PEN is higher than that of TiO_2/PEN at filler content higher than 10 wt%. This phenomenon could be a result of the higher growth rate of their dielectric constant. The efficiencies of both TiO_2/PEN and TiO_2-PEN decrease with the increment of filler content, the same as that of their dielectric loss (Figure S13). Fortunately, the efficiency is still greater than 90%, even at the TiO_2-2CN content of 20 wt%.

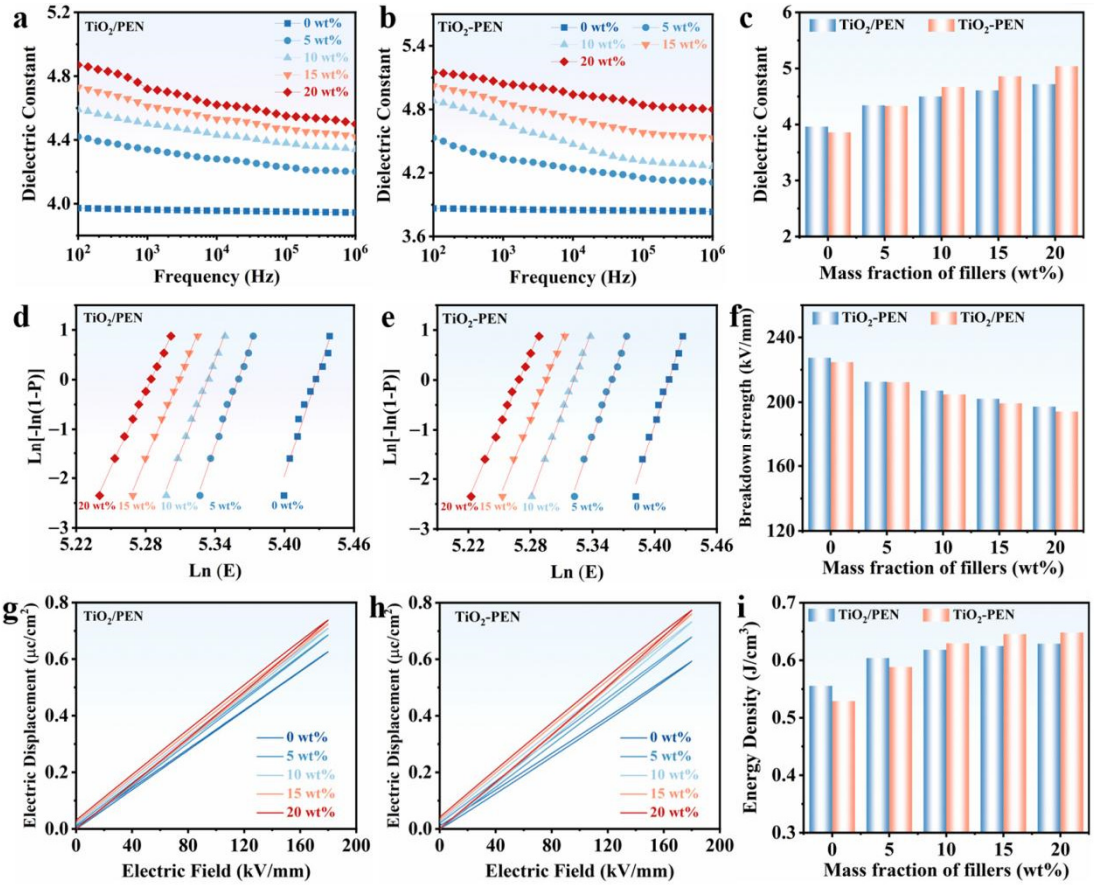

Figure 4. (**a**–**c**) Dielectric constant of TiO_2/PEN and TiO_2-PEN; (**d**–**f**) breakdown strength of TiO_2/PEN and TiO_2-PEN; (**g**,**h**) P-E curves and (**i**) discharged energy density of TiO_2/PEN and TiO_2-PEN.

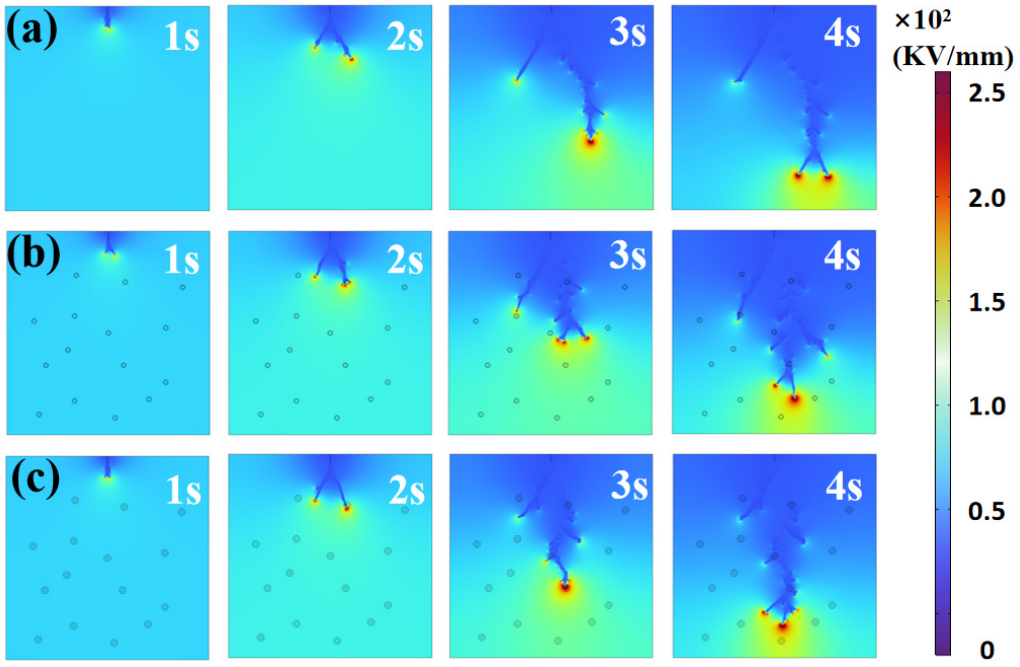

Figure 5. Finite element analysis of the nominal electric potential distribution at various moments during breakdown for different samples. (**a**) PEN-2CN; (**b**) 10 wt% TiO_2/PEN and (**c**) 10 wt% TiO_2-PEN.

Finally, the high-temperature dielectric properties of TiO_2-PEN were detailedly studied. Figure 6a exhibits the dielectric constant of 10 wt% TiO_2-PEN at different temperatures. Similar to the result at room temperature, the dielectric constant of TiO_2-PEN decreases with increasing frequency at high temperature. In addition, as the temperature ascends, TiO_2-PEN dielectric constant at the same frequency also increases gradually. Typically, Figure 6b displays the variation of dielectric constant of TiO_2-PEN from room temperature to 200 °C at 1 kHz. This enhanced dielectric

constant can be attributed to the higher mobility of chain segments and/or polar groups at higher temperatures, which can strengthen the polarization of the system [57]. Nevertheless, this TiO_2-PEN hybrid demonstrates excellent dielectric constant stability within the temperature range as the variation is just 2.7×10^{-7} Hz^{-1}. Figure 6c,d reveals the changes of dielectric loss of 10 wt% TiO_2-PEN at different temperatures, which shows the same phenomena as that of the dielectric constant. The dielectric properties of other TiO_2-PEN hybrids at different temperatures present similar results, as displayed in Figures S14–S21. Furthermore, the breakdown strength and P-E loops of TiO_2-PEN were typically tested at 150 °C. At 150 °C, the breakdown strength of TiO_2-PEN decreases with the increment of TiO_2-2CN (Figure 6e). Moreover, the P-E loops are still linear, while the hysteresis area, representing the loss of energy density, in these loops, becomes larger than that at room temperature (Figure 6g). This can be explained by the increased dielectric loss at high temperatures, which consumes part of the charged energy and converts it into heat. According to the P-E loops, the U_d of TiO_2-PEN at 150 °C is calculated to be 0.54, 0.59, 0.60, 0.61 and 0.62 J/cm^3 when TiO_2-2CN is raised from 0 to 20 wt% (Figure 6i), while the efficiency remains above 85%. Although the U_d of 10 wt% TiO_2-PEN abates with the increased temperature, it maintained 95% of its value at room temperature (0.62 J/cm^3), suggesting excellent thermal stability. In addition, the energy density of TiO_2-PEN at 150 °C could be as high as 0.77, 0.78, 0.79, 0.77, and 0.74 J/cm^3 for 0, 5, 10, 15, and 20 wt% TiO_2-PEN (Figure 6h) basing on the calculation from their dielectric constant and breakdown strength. Furthermore, P-E loops of 10 wt% TiO_2-PEN were cycling measured at 150 °C for 10,000 times. The results show that this TiO_2-PEN hybrid exhibits excellent high-temperature dielectric stability as its U_d and η are maintained even after 10,000 cycling measurements at 150 °C (Figure 6f). Moreover, the dielectric properties of TiO_2-PEN hybrid were compared with those of PEN based composites reported in the literature (Table S3) [58–62]. TiO_2-PEN hybrid fabricated in this work not only shows the highest energy storage density but also demonstrates the highest T_g, which suggests excellent dielectric properties at high temperatures.

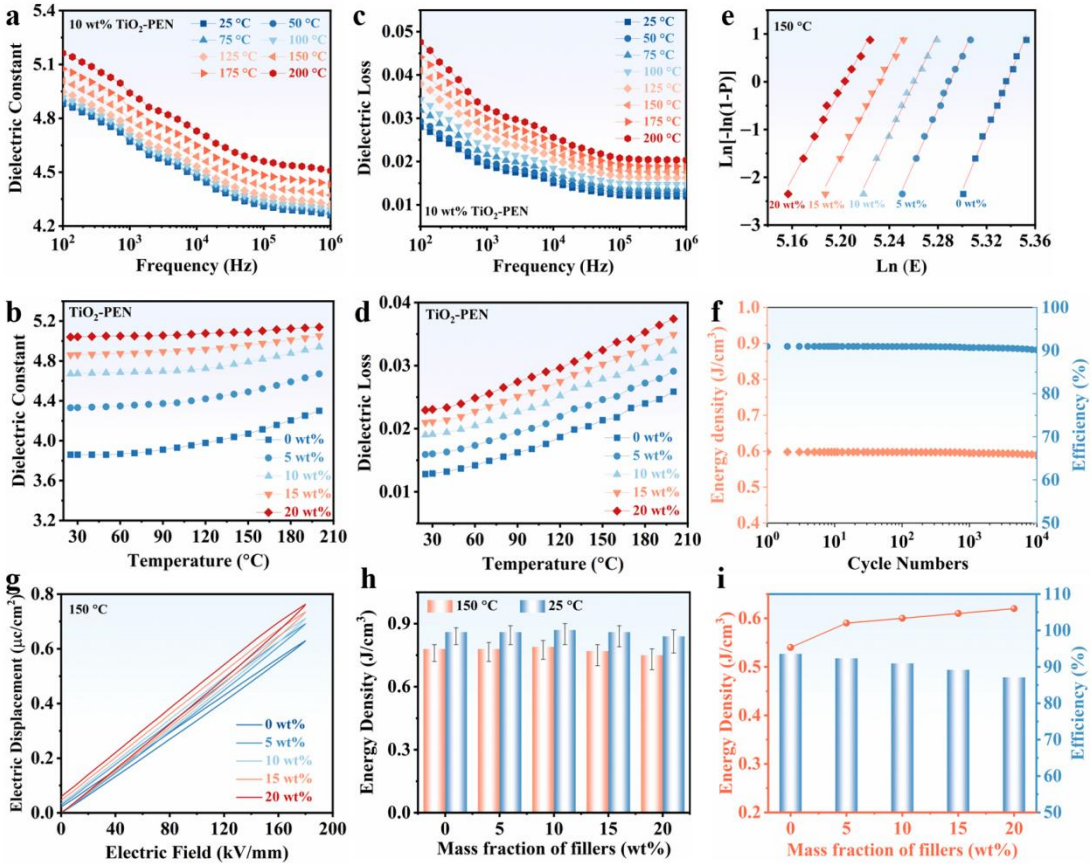

Figure 6. Dielectric constant (**a**) and loss (**c**) of 10 wt% TiO_2-PEN at different temperatures; dielectric constant (**b**) and loss (**d**) of TiO_2-PEN at 1 kHz with the variation of temperature; breakdown strength (**e**) and P-E loops (**g**) of TiO_2-PEN at 150 °C; (**h**) energy density of 10 wt% TiO_2-PEN at 25 and 150 °C; (**i**) U_d and η of TiO_2-PEN at 150 °C; (**f**) U_d and η of 10 wt% TiO_2-PEN at 150 °C during 10,000 times cycling measurement.

4. Conclusions

In summary, TiO_2-PEN hybrids with high-temperature dielectric energy storage properties were fabricated through self-crosslinking of phthalonitriles from TiO_2-2CN and PEN-2CN. Firstly, TiO_2-2CN was synthesized from TiO_2 via a two step procedures using hydrogen peroxide and 4-NPh reactants. After being characterized by FTIR, XRD, TGA, XPS, SEM, and TEM, TiO_2-2CN was introduced into PEN-2CN, preparing TiO_2/PEN nanocomposites by using solution casting method. Finally, TiO_2-PEN hybrids were obtained by treating the TiO_2/PEN nanocomposites at 320 °C for 4 h. The change of SEM sectional morphology, as well as the increasing of T_g and T_d confirmed the successful fabrication of TiO_2-PEN hybrids. Due to the incorporation of fillers, T_g of 10 wt% TiO_2-PEN is enhanced to 218.3 °C, and its U_d reaches 0.63 J/cm^3. In addition, attributing to the formation of covalent bonds in the hybrids, U_d at 150 °C remains 0.60 J/cm^3 for 10 wt% TiO_2-PEN, which is over 95% of that at room temperature. Moreover, the η of this hybrid is higher than 90% and remains unchanged even after 10,000 cycling measurements at 150 °C. The method used for preparing TiO_2-PEN hybrids through self-crosslinking reaction of phthalonitriles provides a new approach to the fabrication of high-temperature dielectric materials.

Supplementary Materials

Summarize the supplementary information with the caption names in this section. The following supporting information can be found at: https://www.sciepublish.com/article/pii/554, Figure S1. DSC curves of TiO_2/PEN nanocomposites. Figure S2. DSC curves of TiO_2-PEN hybrids. Figure S3. TGA curves of TiO_2/PEN nanocomposites. Figure S4. TGA curves of TiO_2-PEN hybrids. Figure S5. Tensile strength of TiO_2/PEN nanocomposites. Figure S6. Tensile modulus of TiO_2/PEN nanocomposites. Figure S7. Elongation at break of TiO_2/PEN nanocomposites. Figure S8. Tensile strength of TiO_2-PEN hybrids. Figure S9. Tensile modulus of TiO_2-PEN hybrids. Figure S10. Elongation at break of TiO_2-PEN hybrids. Figure S11. Dielectric loss of TiO_2/PEN nanocomposites. Figure S12. Dielectric loss of TiO_2-PEN hybrids. Figure S13. Efficiency of TiO_2/PEN nanocomposites and TiO_2-PEN hybrids. Figure S14. Dielectric constant of 0 wt% TiO_2-PEN at different temperatures. Figure S15. Dielectric constant of 5 wt% TiO_2-PEN at different temperatures. Figure S16. Dielectric constant of 15 wt% TiO_2-PEN at different temperatures. Figure S17. Dielectric constant of 20 wt% TiO_2-PEN at different temperatures. Figure S18. Dielectric loss of 0 wt% TiO_2-PEN at different temperatures. Figure S19. Dielectric loss of 5 wt% TiO_2-PEN at different temperatures. Figure S20. Dielectric loss of 15 wt% TiO_2-PEN at different temperatures. Figure S21. Dielectric loss of 20 wt% TiO_2-PEN at different temperatures. Table S1. Properties of TiO_2/PEN nanocomposites. Table S2. Properties of TiO_2-PEN hybrids. Table S3. Comparison of the composites characteristics with those in the literature.

Author Contributions

Methodology, Y.F.; Formal Analysis, S.B., Z.W., Y.L. and Y.J.; Writing—Original Draft Preparation, Y.F.; Writing—Review & Editing, R.W.; Funding Acquisition, L.W., X.H. and R.W.

Ethics Statement

Not applicable.

Informed Consent Statement

Not applicable.

Data Availability Statement

Data can be provided upon request.

Funding

This research was funded by Natural Science Foundation of Shaanxi Province (2024-JC-YBQN-0140) and Key R&D Program Projects in Shaanxi Province (2023JBGS-22).

Declaration of Competing Interest

The authors declare that they have no known competing financial interests or personal relationships that could have appeared to influence the work reported in this paper.

References

1. Wang G, Lu Z, Li Y, Li L, Ji H, Feteira A, et al. Electroceramics for High-Energy Density Capacitors: Current Status and Future Perspectives. *Chem. Rev.* **2021**, *21*, 6124–6172.
2. Pan H, Li F, Liu Y, Zhang Q, Wang M, Lan S, et al. Ultrahigh-energy density lead-free dielectric films via polymorphic nanodomain design. *Science* **2019**, *365*, 578–582.
3. Wu H, Zhuo F, Qiao H, Venkataraman LK, Zheng M, Wang S, et al. Polymer-/ceramic-based dielectric composites for energy storage and conversion. *Energy Environ. Sci.* **2022**, *5*, 486–514.
4. Zubairi H, Lu Z, Zhu Y, Reaney IM, Wang G. Current development, optimisation strategies and future perspectives for lead-free dielectric ceramics in high field and high energy density capacitors. *Chem. Soc. Rev.* **2024**, *53*, 10761–10790.
5. Yang M, Guo M, Xu E, Ren W, Wang D, Li S, et al. Polymer nanocomposite dielectrics for capacitive energy storage. *Nat. Nanotechnol.* **2024**, *19*, 588–603.
6. Qian J, Yu Z, Ge G, Bai H, Lin J, Wei Y, et al. Topological vortex domain engineering for high dielectric energy storage performance. *Adv. Energy Mater.* **2024**, *14*, 2303409.
7. Wang Y, Bao Z, Ding S, Jia J, Dai Z, Li Y, et al. γ-Ray irradiation significantly enhances capacitive energy storage performance of polymer dielectric films. *Adv. Mater.* **2024**, *36*, 2308597.
8. Guo M, Jiang J, Shen Z, Lin Y, Nan C, Shen Y. High-energy-density ferroelectric polymer nanocomposites for capacitive energy storage: enhanced breakdown strength and improved discharge efficiency. *Mater. Today* **2019**, *29*, 49–67.
9. Drakopoulos SX, Wu J, Maguire SM, Srinivasan S, Randazzo K, Davidson EC, et al. Polymer nanocomposites: Interfacial properties and capacitive energy storage. *Prog. Polym. Sci.* **2024**, *156*, 101870.
10. Li X, Hu P, Jiang J, Pan J, Nan C, Shen Y. High-temperature polymer composite dielectrics: energy storage performance, large-scale preparation, and device design. *Adv. Mater.* **2025**, *37*, 2411507.
11. Gurnani R, Shukla S, Kamal D, Wu C, Hao J, Kuenneth C, et al. AI-assisted discovery of high-temperature dielectrics for energy storage. *Nat. Commun.* **2024**, *15*, 6107.
12. Zhou J, Dabaghian M, Wang Y, Sotzing M, LaChance A, Shen K, et al. High-temperature dielectric energy storage films with self-co-assembled hot-electron blocking nanocoatings. *Nano Energy* **2024**, *120*, 109184.
13. Liu X, Zheng M, Chen G, Dang Z, Zha J. High-temperature polyimide dielectric materials for energy storage: theory, design, preparation and properties. *Energy Environ. Sci.* **2022**, *15*, 56–81.
14. Lin M, Zhuo J, Huang S, Zhang Q, Zhang Q. Sandwich-structured polymer dielectrics exhibiting significantly improved capacitive performance at high temperatures by roll-to-roll physical vapor deposition. *Chem. Eng. J.* **2024**, *498*, 155586.
15. Shaver AT, Yin K, Borjigin H, Zhang W, Choudhury SR, Baer E, et al. Fluorinated poly(arylene ether ketone)s for high temperature dielectrics. *Polymer* **2016**, *83*, 199–204.
16. You Y, Liu S, Tu L, Wang Y, Zhan C, Du X, et al. Controllable fabrication of poly (arylene ether nitrile) dielectrics for thermal-resistant film capacitors. *Macromolecules* **2019**, *52*, 5850–5859.
17. Zhang T, Chen X, Thakur Y, Lu B, Zhang Q, Runt J, et al. A highly scalable dielectric metamaterial with superior capacitor performance over a broad temperature. *Sci. Adv.* **2020**, *6*, eaax6622.
18. Azizi A, Gadinski MR, Li Q, Abu AlSaud M, Wang J, Wang Y, et al. High-performance polymers sandwiched with chemical vapor deposited hexagonal boron nitrides as scalable high-temperature dielectric materials. *Adv. Mater.* **2017**, *29*, 1701864.
19. Ren L, Li H, Xie Z, Ai D, Zhou Y, Liu Y, et al. High-temperature high-energy-density dielectric polymer nanocomposites utilizing inorganic core-shell nanostructured nanofillers. *Adv. Energy Mater.* **2017**, *11*, 2101297.
20. Dong J, Hu R, Xu X, Chen J, Niu Y, Wang F, et al. A facile in situ surface-functionalization approach to scalable laminated high-temperature polymer dielectrics with ultrahigh capacitive performance. *Adv. Funct. Mater.* **2021**, *31*, 2102644.
21. Yang M, Zhao Y, Yan H, Wang Z, Xu C, Zhang C, et al. Electrostatic interaction bridges the charge transport kinetics and high-temperature capacitive energy storage performance of polymer dielectrics. *Energy Environ. Sci.* **2024**, *17*, 7627–7648.
22. Li H, Zhou Y, Liu Y, Li L, Li Y, Wang Q. Dielectric polymers for high-temperature capacitive energy storage. *Chem. Soc. Rev.* **2021**, *501*, 6369–6400.
23. Li Q, Yao F, Liu Y, Zhang G, Wang H, Wang Q. High-temperature dielectric materials for electrical energy storage. *Annu. Rev. Mater. Res.* **2018**, *48*, 219–243.
24. Wang L, Wei R, Liu C, Liu X, Li D. Construction of alternating multilayer films with stable absorption-dominated electromagnetic shielding performance and reinforced mechanical properties via interface engineering. *Compos. Part A* **2024**, *176*, 107862.
25. Xiao Q, Han W, Yang R, You Y, Wei R, Liu X. Mechanical, dielectric, and thermal properties of polyarylene ether nitrile and

boron nitride nanosheets composites. *Polymer Composites* **2018**, *39 (S3)*, E1598–E1605.
26. Wei R, Liu K, Liu Y, Wang Z, Jiao Y, Huo Q, et al. Controlled distribution of MXene on the pore walls of polyarylene ether nitrile porous films for absorption-dominated electromagnetic interference shielding materials. *Small* **2025**, *21*, 2407142.
27. Li Q, Chen L, Gadinski M, Zhang S, Zhang G, Li H, et al. Flexible high-temperature dielectric materials from polymer nanocomposites. *Nature* **2016**, *112*, 536.
28. Li H, Gadinski MR, Huang Y, Ren L, Zhou Y, Ai D, et al. Crosslinked fluoropolymers exhibiting superior high-temperature energy density and charge-discharge efficiency. *Energy Environ. Sci.* **2020**, *13*, 1279–1286.
29. Chen S, Meng G, Kong B, Xiao B, Wang Z, Jing Z, et al. Asymmetric alicyclic amine-polyether amine molecular chain structure for improved energy storage density of high-temperature crosslinked polymer capacitor. *Chem. Eng. J.* **2020**, *387*, 123662.
30. Tang Y, Xu W, Niu S, Zhang Z, Zhang Y, Jiang Z. Crosslinked dielectric materials for high-temperature capacitive energy storage. *J. Mater. Chem. A* **2021**, *9*, 10000–10011.
31. Zhu L, Zhang Y, Xu W, Zhu X, Niu S, Zhang Y, et al. Crosslinked polyetherimide nanocomposites with superior energy storage achieved via trace Al_2O_3 nanoparticles. *Compos. Sci. Technol.* **2022**, *223*, 109421.
32. Zhu L, Zheng Z, Xu W, Tang Y, Yao H, Zhang Y, et al. Optimizing high-temperature capacitive energy storage performance by constructing crosslinked structure in self-crosslinkable polyetherimides. *Mater. Today Energy* **2022**, *30*, 101145.
33. Wang Z, Wei R, Liu X. Preparation and dielectric properties of copper phthalocyanine/graphene oxide nanohybrids via in situ polymerization. *J. Mater. Sci.* **2016**, *51*, 4682–4690.
34. Tu L, Xiao Q, Wei R, Liu X. Fabrication and enhanced thermal conductivity of boron nitride and polyarylene ether nitrile hybrids. *Polymers* **2019**, *11*, 1340.
35. Wei R, Liu Y, Gao F, Feng Z, Huo Q, Liu K, et al. Enhancing high-temperature energy storage performance of poly (arylene ether nitrile) hybrids synergistically via phthalonitrile modified boron nitride and carbon nanotube. *Adv. Compos. Hybrid Mater.* **2024**, *7*, 50.
36. Yang R, Wei R, Li K, Tong L, Jia K, Liu X. Crosslinked polyarylene ether nitrile film as flexible dielectric materials with ultrahigh thermal stability. *Sci. Rep.* **2016**, *6*, 36434.
37. Wei R, Zhan C, Yang Y, He P, Liu X. Polyarylene ether nitrile and titanium dioxide hybrids as thermal resistant dielectrics. *Chin. J. Polym. Sci.* **2021**, *39*, 211–218.
38. Kumar PM, Badrinarayanan S, Sastry M. Nanocrystalline TiO_2 studied by optical, FTIR and X-ray photoelectron spectroscopy: correlation to presence of surface states. *Thin Solid Film.* **2000**, *358*, 122–130.
39. Zharnikova N, Usol'tseva N, Kudrik E, Thelakkat M. Synthesis, mesomorphism and electrochemical properties of tetrasubstituted zinc and copper phthalocyanines. *J. Mater. Chem.* **2009**, *19*, 3161–3167.
40. Zhang Z, Zhou L, Wang L, Hao Q, Hua X, Wei R. Enhancing energy storage density of poly(arylene ether nitrile) via incorporating modified barium titanate nanorods and hot-stretching. *Nano Res.* **2024**, *17*, 7574–7584.
41. Xie K, Ren K, Wang Q, Lin Y, Ma F, Sun C, et al. In situ construction of zinc-rich polymeric solid-electrolyte interface for high-performance zinc anode. *eScience* **2023**, *3*, 100153.
42. Wang L, Feng Z, Hou Q, Dang Z, Yu Y, Yang C, et al. Quaternary ammonium salt functionalized copper phthalocyanine-graphene oxide hybrids for cocatalyst-free carbon dioxide cycloaddition. *Adv. Compos. Hybrid Mater.* **2025**, *8*, 40.
43. Zhang J, Li M, Feng Z, Chen J, Li C. UV Raman spectroscopic study on TiO_2: I.: Phase transformation at the surface and in the bulk. *J. Phys. Chem. B* **2006**, *110*, 927–935.
44. Gao F, Zhou L, Liu K, Feng Z, Huo Q, Yang C, et al. Improving energy storage properties of polyarylene ether nitrile with coral-like $CaCu_3Ti_4O_{12}$ nanorods. *Chem. Eng. J.* **2024**, *493*, 152830.
45. Liu Y, Tang B, Wang Z, Jiao Y, Hou Q, Dang Z, et al. Enhanced dielectric performances of strontium barium titanate nanorod composites via improved interfacial compatibility. *J. Colloid Interface Sci.* **2025**, *680*, 85–95.
46. Zhou L, Zhang Z, Feng Y, Gao F, Luo Y, Li S, et al. Covalently cross-linked $CaCu_3Ti_4O_{12}$ and poly (arylene ether nitrile) hybrids with enhanced high temperature energy storage properties. *Mater. Today Commun.* **2024**, *38*, 108544.
47. Bianchi O, Oliveira RVB, Fiorio R, Martins JDN, Zattera AJ, Canto LB. Assessment of Avrami, Ozawa and Avrami-Ozawa equations for determination of EVA crosslinking kinetics from DSC measurements. *Polym. Test.* **2008**, *27*, 722–729.
48. Rhim JW, Park HB, Lee CS, Jun JH, Kim DS, Lee YM. Crosslinked poly(vinyl alcohol) membranes containing sulfonic acid group: proton and methanol transport through membranes. *J. Membr. Sci.* **2004**, *238*, 143–151.
49. Krumova M, López D, Benavente R, Mijangos C, Pereña JM. Effect of crosslinking on the mechanical and thermal properties of poly(vinyl alcohol). *Polymer* **2000**, *41*, 9265–9272.
50. Wei R, Li K, Ma J, Zhang H, Liu X. Improving dielectric properties of polyarylene ether nitrile with conducting polyaniline. *J. Mater. Sci. Mater. Electron.* **2016**, *27*, 9565–9571.
51. Fabiani D, Simoni L. Discussion on application of the Weibull distribution to electrical breakdown of insulating materials. *IEEE Trans. Dielectr. Electr. Insul.* **2005**, *12*, 11–16.
52. Chaitanya Pitike K, Hong W. Phase-field model for dielectric breakdown in solids. *J. Appl. Phys.* **2014**, *115*, 044101.
53. Duan G, Hu F, Zhang R, Hu Z. Preparation of a novel cross-linked polyetherimide with enhanced breakdown strength and

high-temperature energy storage performance. *High Volt.* **2023**, *8*, 630–639.
54. Wei R, Tu L, You Y, Zhan C, Wang Y, Liu X. Fabrication of crosslinked single-component polyarylene ether nitrile composite with enhanced dielectric properties. *Polymer* **2019**, *161*, 162–169.
55. Tu L, You Y, Liu C, Zhan C, Wang Y, Cheng M, et al. Enhanced dielectric and energy storage properties of polyarylene ether nitrile composites incorporated with barium titanate nanowires. *Ceram. Int.* **2019**, *45*, 22841–22848.
56. Pei J, Yin L, Zhong S, Dang Z. Suppressing the loss of polymer-based dielectrics for high power energy storage. *Adv. Mater.* **2023**, *35*, 2203623.
57. Jiang J, Li J, Zhang Y, Yuan Y, Liu X, Zuo P, et al. Tuning the interfacial insulating shell characteristics in $CaCu_3Ti_4O_{12}$ nanowires/polyetherimide nanocomposites for high-temperature capacitive energy storage. *J. Mater. Chem. C* **2022**, *10*, 7962–7969.
58. Gao F, Wei R, Zhou L, Luo W, Li Z, Pang L, et al. Improved dielectric properties of poly(arylene ether nitrile) with sulfonated poly(arylene ether nitrile) modified $CaCu_3Ti_4O_{12}$. *Polym. Compos.* **2023**, *44*, 8658–8668.
59. Hu W, You Y, Tong L, Tu L, Wang Y, Wei R, et al. Preparation and physical properties of polyarylene ether nitrile and polyarylene ether sulfone random copolymers. *High Perform. Polym.* **2018**, *31*, 686–693.
60. Mao H, You Y, Tong L, Tang X, Wei R, Liu X. Dielectric properties of deblock copolymers containing a polyarylene ether nitrile block and a polyarylene ether ketone block. *J. Mater. Sci. Mater. Electron.* **2017**, *29*, 3127–3134.
61. You Y, Han W, Tu L, Wang Y, Wei R, Liu X. Double-layer core/shell-structured nanoparticles in polyarylene ether nitrile-based nanocomposites as flexible dielectric materials. *RSC Adv.* **2017**, *7*, 29306–29311.
62. Wei R, Huo Q, Liu K, Elnaggar AY, El-Bahy SM, El-Bahy ZM, et al. Distributing fluorinated carbon nanotube on pore walls of polyarylene ether nitrile porous films for advanced electromagnetic interference shielding. *Adv. Compos. Hybrid Mater.* **2024**, *7*, 196.